CrossMark

Radiation decay of thaumatin crystals at three X-ray energies

## Dorothee Liebschner,[a] Gerold Rosenbaum,[b] Miroslawa Dauter[c] and Zbigniew Dauter[d]*

[a]Structural Biology Research Center, Photon Factory, Institute of Materials Structure Science, High Energy Accelerator Research Organization, Tsukuba, Japan, [b]Department of Biochemistry, University of Georgia and Structural Biology Center, Argonne National Laboratory, Argonne, IL 60439, USA, [c]Leidos Biomedical Research Inc., Basic Science Program, Argonne National Laboratory, Argonne, IL 60439, USA, and [d]Synchrotron Radiation Research Section, MCL, National Cancer Institute, Argonne National Laboratory, Argonne, IL 60439, USA. *Correspondence e-mail: dauter@anl.gov

Radiation damage is an unavoidable obstacle in X-ray crystallographic data collection for macromolecular structure determination, so it is important to know how much radiation a sample can endure before being degraded beyond an acceptable limit. In the literature, the threshold at which the average intensity of all recorded reflections decreases to a certain fraction of the initial value is called the 'dose limit'. The first estimated D_{50} dose-limit value, at which the average diffracted intensity was reduced to 50%, was 20 MGy and was derived from observing sample decay in electron-diffraction experiments. A later X-ray study carried out at 100 K on ferritin protein crystals arrived at a D_{50} of 43 MGy, and recommended an intensity reduction of protein reflections to 70%, D_{70}, corresponding to an absorbed dose of 30 MGy, as a more appropriate limit for macromolecular crystallography. In the macromolecular crystallography community, the rate of intensity decay with dose was then assumed to be similar for all protein crystals. A series of diffraction images of cryocooled (100 K) thaumatin crystals at identical small, 2° rotation intervals were recorded at X-ray energies of 6.33 , 12.66 and 19.00 keV. Five crystals were used for each wavelength. The decay in the average diffraction intensity to 70% of the initial value, for data extending to 2.45 Å resolution, was determined to be about 7.5 MGy at 6.33 keV and about 11 MGy at the two higher energies.

1. Introduction

X-ray photons, which give rise to the diffraction patterns used for structure determination, are also absorbed by the crystalline sample, thus creating a cascade of damaging processes. As a consequence, the structure of the sample changes, accompanied by a change in the diffraction intensities, as reported early on by Blake & Phillips (1962). In contrast to the individual diffraction intensities, which may increase or decrease, the average intensity monotonically decreases as the X-ray dose increases. At a certain level of decay, structure solution and biological interpretation become unreliable (Blake & Phillips, 1962; Hendrickson, 1976; Garman & Nave, 2002; Ravelli & Garman, 2006; Holton, 2009; Garman, 2010).

Besides the global decay of average diffraction intensities, specific structural changes occur, such as the breakage of disulfide bonds and the decarboxylation of glutamates and aspartates (Burmeister, 2000; Weik et al., 2000; Ravelli & McSweeney, 2000). Although we do not analyze site-specific decay in this report, it should be noted that these local structural changes have been observed at much lower doses than those that induce noticeable global decay (Ravelli & McSweeney, 2000; Weik et al., 2000). The review by Garman
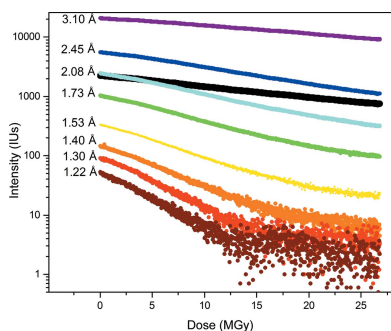
Table 1
Experimental conditions at the three different photon energies.

Crystal	Rotation (°)	Exposure time† (s)	Detector distance (mm)	No. of images	Maximum resolution (Å)
6.33 keV (1.959 Å)					
xtal01	2	2	108	250	2.08
xtal02					
xtal03					
xtal04					
xtal05					
12.66 keV (0.979 Å)					
xtal01	2	2	150	1000	1.22
xtal02					
xtal03‡					
xtal04					
xtal05					
19.00 keV (0.653 Å)					
xtal01	2	5 (20)	230	200	1.22
xtal02		5 (20)			
xtal03		5 (20)			
xtal04		4 (16)			
xtal05		4 (16)			

† For 19 keV, the times in parentheses denote the exposure times for the unrecorded 'burn'. ‡ xtal03 at 12.66 keV was not used in the analysis since it moved partially out of the beam during the experiment.

(2010) provides an informative introduction to radiation damage in crystals of biological macromolecules. Apart from the global decay of intensities, other effects of radiation damage that can be readily derived from diffraction images are changes in unit-cell parameters, mosaicity and scaling B factors. However, apart from the B factors (Kmetko *et al.*, 2006), they are not useful as metrics for radiation damage.

Cooling crystals to cryogenic temperatures extends their lifetime by a factor of 20–50 (Hope, 1988; Rodgers, 1994; Kmetko *et al.*, 2006; Warkentin & Thorne, 2010; Warkentin *et al.*, 2013). However, the very high fluxes available at third-generation storage rings make it possible to record diffraction data from more weakly diffracting samples, or at a higher resolution, in a reasonably short time, resulting in high radiation doses. For these reasons, radiation-damage research has again become a major concern in the biocrystallographic community. The first quantitative estimation of radiation damage was provided *via* electron-diffraction experiments performed by Henderson (1990), who estimated that the dose of energy absorbed by crystalline samples that diminished the average intensity of diffracted reflections to 50%, D_{50}, equaled 20 MGy. He proposed this value as a dose limit for X-ray crystallography on cryocooled protein crystals. The results obtained by Owen *et al.* (2006) on the basis of X-ray diffraction data collected at 100 K from ferritin crystals suggested a D_{50} value of 43 MGy. These authors suggested that a more appropriate criterion for the radiation-damage limit is D_{70}, the dose value that lowers the average intensity to $\ln(2) \simeq 0.70$. The value $D_{70} = 30$ MGy is usually referred to as the 'Garman limit'.

Since June 1999, regular biannual meetings have summarized current research on X-ray radiation damage to biological samples (International Workshop on X-ray Radiation Damage to Biological Crystalline Samples, 1999–2014) and their proceedings have been published in special issues of the

Journal of Synchrotron Radiation (volume 9, part 6; volume 12, part 3; volume 14, part 1; volume 16, part 2; volume 18, part 3; volume 20, part 1).

While investigating the relation between diffraction data quality and photon energy, we noticed that the reflection intensities measured from crystals of thaumatin decayed with dose significantly more rapidly than expected. Thus, we decided to study these observations in more detail, since they suggested that there may be no generally applicable radiation-dose limit and that different crystals may have different susceptibilities to radiation damage.

We recorded a series of diffraction images at identical 2° rotation intervals at three different energies (6.33, 12.66 and 19.00 keV) and analyzed the data in terms of radiation damage. For each photon energy, we collected data from five different samples using the same protocol in order to ensure a certain degree of statistical validity of the results and to average the variations between individual samples.

2. Materials and methods

2.1. Crystallization and data collection

Thaumatin was chosen as a test protein because it is easily available and crystallizes readily. Crystals were grown by the hanging-drop method using a protein solution at approximately 35 mg ml^{-1} in 50 mM HEPES buffer pH 7.0 mixed in a 1:1 ratio with well solution consisting of 0.75 M sodium/potassium tartrate, 0.1 M citrate buffer pH 6.5. For data collection, the crystals were cooled in a stream of gaseous nitrogen at 100 K delivered by an Oxford Cryosystems cryocooler. The cryosolution consisted of reservoir solution supplemented with 28%(v/v) glycerol and all crystals were briefly immersed (for 3–5 s) in it before being rapidly transferred to a goniostat. All crystals were tetragonal, belonging to space group $P4_12_12$, with unit-cell parameters of about $a = b = 58$, $c = 150$ Å.

Diffraction data were collected on beamline 19-ID of the Structural Biology Center at the Advanced Photon Source (APS), Argonne National Laboratory (Rosenbaum *et al.*, 2006) using an ADSC Q315r CCD detector at X-ray energies of 19.00, 12.66 and 6.33 keV. The long c cell dimension of each crystal was oriented approximately parallel to the detector plane in order to avoid overlap of reflection profiles on the detector. Diffraction images with the same starting crystal orientation and a rotation width of 2° were recorded consecutively. This method of recording a series of diffraction images at identical small rotation intervals guarantees that the same crystal volume is always irradiated and minimizes the influence of the properties of the crystal and detector on the relative accuracy of recorded diffraction intensities of consecutive images (Liebschner *et al.*, 2012; Sliz *et al.*, 2003). The exposure time per frame was selected to keep the number of overloaded detector pixels at less than 40 in the first image. The total number of images was adjusted to the lifetime of the crystal, *i.e.* consecutive frames were recorded until the high-resolution spots disappeared. At 19 keV, this procedure would

Table 2
Parameters relevant for calculation of the dose with *RADDOSE* v.2 (Paithankar *et al.*, 2009).

Crystal	Flux for first image (10^{10} photons s^{-1})	Beam size† (µm)	Crystal dimensions‡ (µm)	Dose for first image (MGy)
6.33 keV (1.959 Å)				
xtal01	12.0	75, 92	111, 113, 87	0.068
xtal02	11.7		105, 152, 99	0.065
xtal03	12.3		131, 133, 100	0.069
xtal04	12.2		110, 107, 126	0.066
xtal05	11.7		98, 112, 119	0.064
12.66 keV (0.979 Å)				
xtal01	4.5	51, 29	99, 145, 120	0.031
xtal02	5.4		101, 86, 93	0.038
xtal04	5.4		111, 120, 116	0.038
xtal05	5.2		103, 107, 96	0.037
19.0 keV (0.653 Å)				
xtal01	5.7	44, 39	147, 125, 112	0.036
xtal02	5.8		136, 100, 80	0.036
xtal03	5.8		111, 107, 129	0.037
xtal04	5.8		138, 103, 113	0.029
xtal05	5.7		144, 125, 113	0.029

† The beam size is given as the horizontal dimension followed by the vertical dimension. ‡ The crystal dimensions are given as horizontal, vertical and thickness values.

have led to a very large number of exposures before the crystals were exhausted. Therefore, a protocol consisting of a recorded exposure of 4 or 5 s followed by a four times longer unrecorded 'burn' exposure with the same X-ray flux was used. At 6.33 keV, the X-ray beam was attenuated by a 0.08 mm thick aluminium sheet (13% transmission) in order to use an exposure time similar to that used for the other energies without creating too many overloaded pixels. Table 1 summarizes the experimental conditions for each crystal at each wavelength.

2.2. Dose calculation

The dose was estimated using *RADDOSE* v.2 (Paithankar *et al.*, 2009). Table 2 summarizes the relevant dose-calculation parameters of the experiment, such as crystal dimensions, beam size and flux.

We used the horizontal and vertical focusing elements to form the beam profile into as rectangular ('top hat') a shape as possible in order to achieve a dose across the irradiated crystal volume that was as uniform as possible. Fig. 1 shows the typical horizontal and vertical beam profiles used, recorded by scanning a 13 µm wide slit across the beam. The X-ray flux was measured using a dry, nitrogen-filled ionization chamber with an active length of 100 mm. The recorded current was converted to the rate of incident photons using tabulated mass absorption coefficients of nitrogen (McMaster *et al.*, 1969), assuming standard density and a work function of 34.6 eV per electron–ion pair. For validation, a 12.6 keV X-ray flux measured with the ion chamber was compared with the same flux measured with a calibrated Si PIN diode [DP00325, calibrated, with an uncertainty of 1%, by the Physikalisch-Technische Bundesanstalt (PTB), Germany; on loan from the APS Detector Pool] and found to be in agreement within 5%. The flux at the sample was derived from the flux measured

with the ion chamber by correcting for all absorption between the location of the sample and the location of the collector plates in the ion chamber.

At low photon energies, absorption becomes noticeable and the flux along the beam path through the crystal can no longer be assumed to be constant. At 6.33 keV, the absorption of
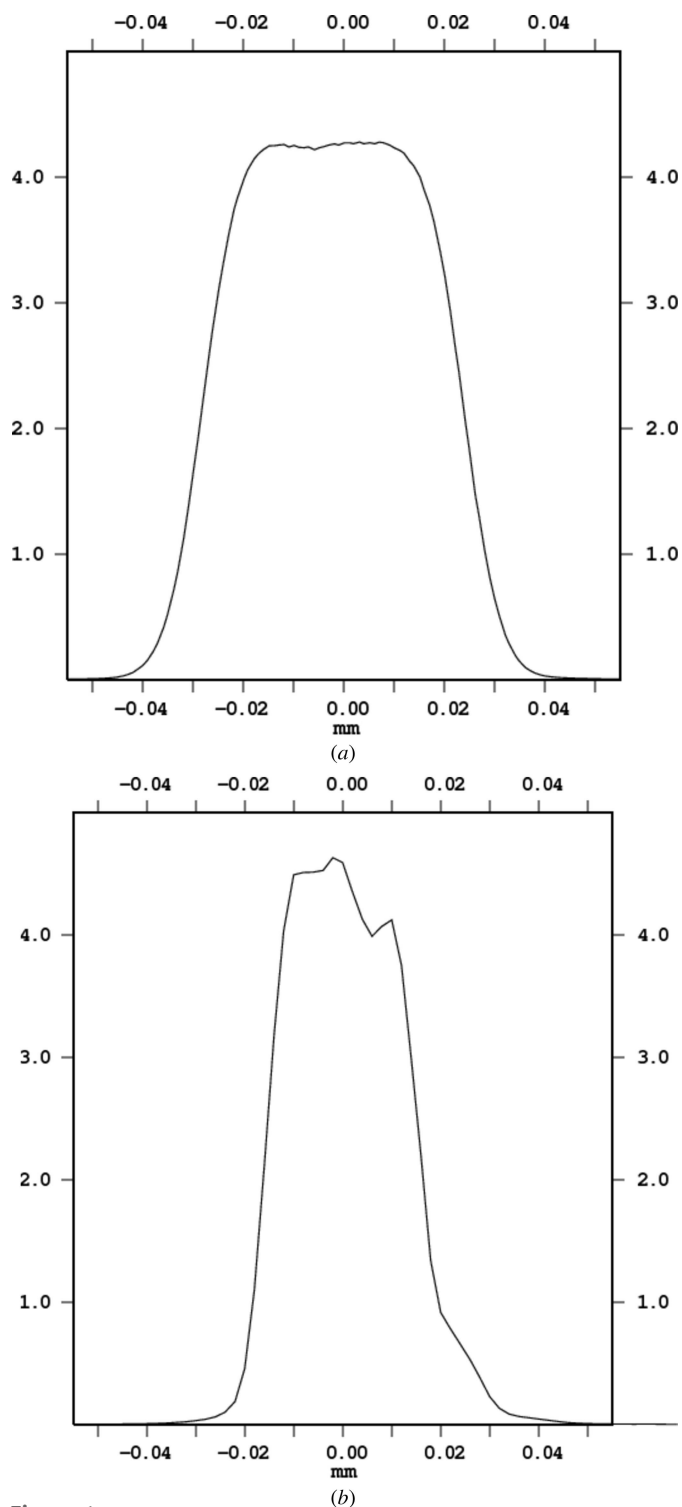

Figure 1
Horizontal (*a*) and vertical (*b*) profiles of the beam used for the experiment at 12.66 keV. The vertical scale of the intensities is arbitrary. The beam profiles at 6.33 and 19.0 keV were very similar.

water (a reasonable surrogate for a protein crystal) is about 19% per 0.1 mm thickness. The resulting dose gradient is taken into account by *RADDOSE* as it calculates an average dose. It should be noted that the dose gradient adds to the uncertainty in the dose calculation as the three-dimensional shape of the crystal is only approximately known and is not an input parameter to *RADDOSE*. Not taken into account is the solvent layer in front of the crystal. Using pictures of the mounted samples, we determined the approximate thickness of the solvent layer, calculated the absorption coefficient of the solvent (using the web server at http://henke.lbl.gov/optical_constants/) and corrected the flux accordingly. The possible inaccuracy of at most 20 µm in the visual estimation of the solvent and crystal thickness may result in an uncertainty in the dose of 5% at 6.33 keV. At 12.66 and 19 keV, absorption is so small that these corrections would not be significant. The overall uncertainties in the dose estimations are therefore about 5% for 12.66 and 19 keV and not more than 10% for 6.33 keV.

The small changes in flux on the sample that occurred during the course of the exposure series were recorded by a beam-position/beam-intensity monitor (BPM; Alkire *et al.*, 2000) located downstream of the collimating slits. The beam-intensity signal from the BPM that had been referenced against the ion-chamber current for each photon energy was used to adjust the dose value assigned to each image relative to the dose calculated for the first image.

2.3. Data analysis

The diffracted intensities were integrated with *DENZO* (Otwinowski & Minor, 1997) using the 'oscillation start X' command, which prevents the program from advancing the crystal rotation matrix between consecutive exposures. Furthermore, the mosaicity was deliberately overestimated and fixed to 0.5° for each image in order to safely classify reflections marked as fully recorded ('fullys'). In addition,
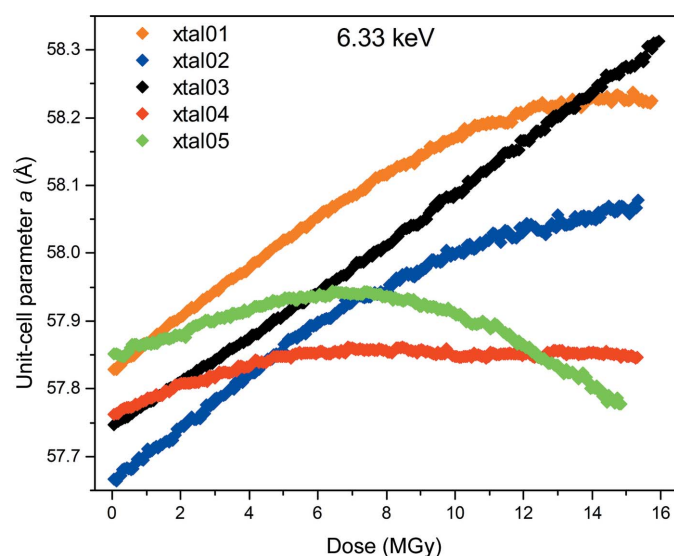

Figure 2
Change of the unit-cell parameter *a* as a function of dose for the five crystals measured at 6.33 keV. The color code is indicated at the top left.

since the unit-cell parameters of the crystals changed slightly with increasing dose (Fig. 2), we made sure that for each crystal only reflections that were fully recorded and present in all images were included in calculations. The intensities obtained from profile fitting and stored in the individual output *.x files of each image were used for further analysis. The Lorentz and polarization corrections were not applied in the estimation of reflection intensities, since this analysis focused on the decay of diffracted intensities not structure-factor amplitudes. Average intensities were computed for the whole resolution range and in smaller resolution shells; the same limits were applied for all crystals at each energy.

3. Results and discussion

3.1. Overall properties of the data sets

The experiment yielded 15 sets of 2° rotation images, with each set containing essentially the same reflections in each diffraction frame. As a result of the slowly changing mosaicity and unit-cell parameters, the images differed slightly in the occurrence of the partially recorded reflections. In the analysis, however, only reflections classified as safe 'fullys' were used. The only differences between the intensities of fully recorded reflections in consecutive images stem from decay owing to radiation damage. Integration of the data with *DENZO* was successful and all fully recorded intensities from the output *.x files were analyzed in terms of radiation damage. However, after preliminary examination of the intensities, it was determined that xtal03 at 12.66 keV probably slipped during data collection, so the data from this crystal were not used in this study.

The resolution of the data recorded at 12.66 and 19.0 keV extended to 1.22 Å; however, at 6.33 keV the minimum detector distance of 108 mm limited the resolution to 2.08 Å, even though the crystals were of good quality and would certainly have diffracted to higher resolution.

Table 2 lists the parameters relevant to the dose calculation (flux, beam size and crystal size) and the dose that the crystals received during the measurement of the first image of each series. The doses of the following images were prorated according to the small changes in flux recorded by the method described in §2.2.

3.2. Decay of average intensities

Fig. 3 shows the decay of the average intensity as a function of dose for the data sets recorded at 19.0 keV, calculated for the whole resolution range, which was 30–1.22 Å at this energy. The curves are very smooth and do not display any discontinuities. The five crystals have different average intensities in the beginning, ranging from 2250 integrated units (IUs; *i.e.* the units of *DENZO* *.x files) for xtal04 to over 4000 IUs for xtal01. They decay to less than 700 IUs (xtal04) and 900 IUs (xtal01) after recording 200 images, which is far beyond the extent of decay investigated in this study. All five curves have the exponential shape observed in the first radiation-damage study by Blake & Phillips (1962).

Table 3
Doses at which the average intensities in the indicated resolution ranges have decayed to 70% (D_{70}) and to 50% (D_{50}) of the initial value.

The last column contains the relative diffractive efficiency of each crystal, derived from the average intensity of reflections recorded in the first image and normalized by flux and irradiated crystal volume. The uncertainty in the dose estimations is about 10% for the 6.33 keV data and about 5% for the other energies.

Energy (keV)	Crystal	D_{70} (MGy) 30–2.45 Å	30–2.08 Å	30–1.22 Å	D_{50} (MGy) 30–2.45 Å	30–2.08 Å	30–1.22 Å	Diffraction efficiency
6.33	xtal01	6.7	6.5		11.6	11.2		2.5
	xtal02	6.7	6.5		11.6	11.2		1.3
	xtal03	8.4	8.0		14.4	13.7		1.8
	xtal04	8.2	7.8		14.7	14.1		1.7
	xtal05	7.5	7.2		12.0	11.6		1.6
	Average	7.5	7.2		12.8	12.4		
12.66	xtal01	12.0	10.7	9.3	22.3	20.6	17.9	2.9
	xtal02	11.5	10.5	9.0	21.6	20.0	17.6	3.4
	xtal04	11.5	10.4	9.2	20.1	18.4	16.7	2.4
	xtal05	9.4	8.5	7.4	17.5	16.0	14.3	1.4
	Average	11.1	10.1	8.8	20.4	18.7	16.6	
19.0	xtal01	11.0	9.6	8.0	20.3	18.3	15.8	3.8
	xtal02	12.1	10.6	8.5	21.2	19.1	16.1	4.3
	xtal03	12.5	11.2	10.1	21.8	20.2	18.6	2.1
	xtal04	10.5	9.3	7.6	17.8	16.2	13.6	2.6
	xtal05	11.0	9.6	8.2	19.0	17.1	14.8	2.9
	Average	11.4	10.0	8.5	20.0	18.2	15.8	

Fig. 4 shows the decay of the average intensity for xtal01 at 12.66 keV in different resolution shells and for the whole resolution range (30.0–1.22 Å). The average intensities decrease monotonically with increasing resolution. Likewise, the slope of the decay increases monotonically with increasing resolution.

By dividing the average intensity of an image by the intensity I_1 recorded in the first image of the exposure series, the dose D_{lim} at which the intensity falls off to a percentage (lim) of its initial value can be readily derived. Table 3
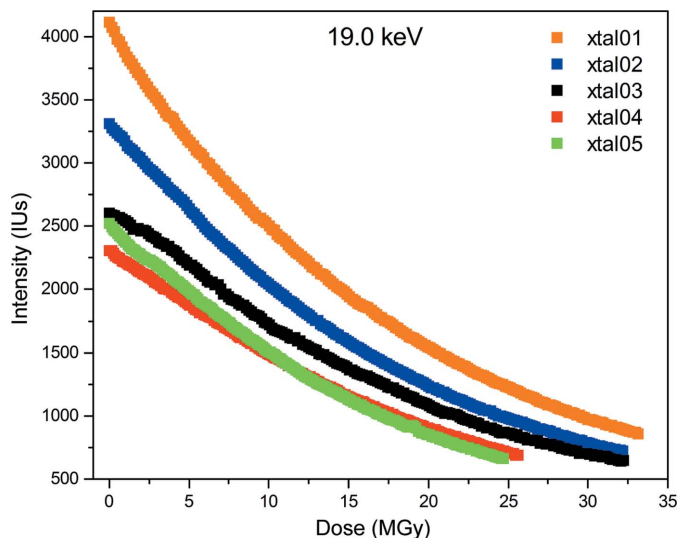
summarizes the values for D_{70}, at which the intensity is reduced to 70% of I_1, and D_{50}, at which the intensity is halved, for data extending to different high-resolution limits: 2.45 Å, comparable to that used by Owen *et al.* (2006); 2.08 Å, the highest resolution limit common to all three energies; and 1.22 Å, the highest achieved limit for 12.66 and 19.0 keV.

For resolutions up to 2.45 Å, the average D_{70} values are 7.5, 11.1 and 11.4 MGy for 6.33, 12.66 and 19.0 keV, respectively. For the resolution range 30–2.08 Å the corresponding values are 7.2, 10.1 and 10.0 MGy. Whereas X-radiation at the two higher energies appears to incur comparable damage to thaumatin crystals, the dose tolerance at the lower photon energy is 30% lower.

Different investigations using various methodologies have reported both energy dependence and independence of radiation damage. Fourme *et al.* (2012) stated that the data-collection efficiency increases about eight times when the photon energy changes from 8 to 30 keV. In contrast, Homer *et al.* (2011) found that site-specific damage at disulfide-bridge sites is greater at 14 keV than at 9 keV, although methionine S atoms display no energy dependence. Shimizu *et al.* (2007) studied radiation damage of HEWL crystals over an energy range from 6.5 to 33 keV. Using criteria such as changes in mosaicity,
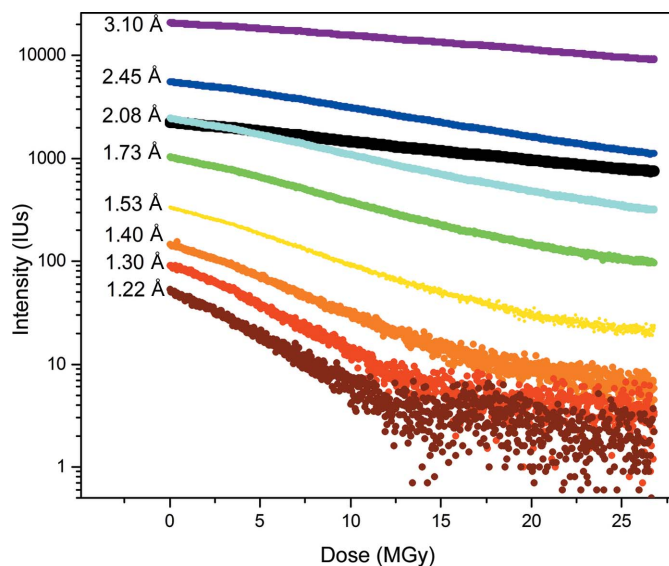

Figure 3
Average intensities as a function of dose for the data recorded at 19.0 keV. A resolution range of 30.0–1.22 Å was used for the calculation. The color code is indicated at the top right.

Figure 4
Mean intensities in different resolution shells as a function of dose for the data from xtal01 recorded at 12.66 keV. The average intensity in the total range is displayed in black. All other curves show the decay for consecutive resolution intervals which are indicated to the left; for example, the resolution range is 30.0–3.10 Å for the top curve (violet) and 3.10–2.45 Å for the second curve (blue).

unit-cell parameters and B factors as a damage metric, they found no clear dependence of damage on photon energy. Weiss *et al.* (2005) observed no significant difference in the radiation damage to crystals of a Cd derivative of elastase at wavelengths of 1.0 and 2.0 Å (12.4 and 6.2 keV, respectively).

Our results indicate that the D_{70} dose limit is about 11 MGy at 12.66 and 19.0 keV, about three times smaller than the value of 30 MGy derived by Owen *et al.* (2006) at the same resolution. We do observe a different D_{70} dose limit of 7.5 MGy at 6.33 keV, which suggests that at low energy (long wavelength) thaumatin crystals are more susceptible to radiation damage. The average D_{50} dose limits are 12.8, 20.4 and 20.0 MGy at 6.33, 12.66 and 19.0 keV, respectively.

In a recent study (Zeldin *et al.*, 2013), D_{50} values varied from 7 to 42 MGy depending on how the dose was estimated. The authors conclude that the 'diffraction-weighted dose' is the most efficient metric, and report a value of 12.9 MGy for insulin crystals at a resolution of 1.8 Å, which is also significantly lower than the value reported by Owen and coworkers.

As a side issue, we noted that the average intensity of reflections in the first image varied by up to a factor of two between the five crystals measured at each X-ray energy. Large variations in diffractive efficiency are often observed when different parts of a crystal are probed with a finely focused beam. Assuming that this is the result of a more perfect crystalline order and considering that one contribution to intensity decay is the corruption of the crystal lattice with increasing dose, it might be interesting to know whether higher diffractive efficiency results in higher dose tolerance. In Table 3, the relative diffractive efficiency derived by normalizing the average intensity of the first image by flux, exposure time and irradiated crystal volume is listed for each crystal. Note that comparison between the calculated values is only valid between crystals measured at the same energy. There seems to be no apparent correlation between diffractive efficiency and the D_{70} or D_{50} doses.

4. Conclusions

Recording a series of diffraction images at the same crystal orientation makes it possible to quantitatively assess the effect of X-ray radiation damage on the intensities of diffracted reflections, simultaneously minimizing the influence of various potential sources of error such as the sphere of confusion of the goniostat, imperfect centering of the crystal, residual non-uniformity of detector response or non-uniformly irradiated crystal volume when integrating over large rotation angles. This experiment, which was conducted on several crystals of thaumatin at three different X-ray energies (6.33, 12.66 and 19.0 keV), resulted in the estimation of the D_{70} dose that reduces the average intensity of reflections to 70% of the initial value. The D_{70} for reflections within a resolution range of 30–2.45 Å was estimated to be about 11 MGy for 12.66 and 19.0 keV radiation and 7.5 MGy for 6.33 keV radiation. These results suggest a D_{70} dose limit that is about three times smaller than the value of 30 MGy estimated by Owen *et al.* (2006) for a similar wavelength and resolution. This study suggests that there is no universally applicable dose limit for all types of protein crystals.

References

Alkire, R. W., Rosenbaum, G. & Evans, G. (2000). *J. Synchrotron Rad.* **7**, 61–68.
Blake, C. C. F. & Phillips, D. C. (1962). *Biological Effects of Ionizing Radiation at the Molecular Level*, pp. 2–6. Vienna: International Atomic Energy Agency.
Burmeister, W. P. (2000). *Acta Cryst.* D**56**, 328–341.
Fourme, R., Honkimäki, V., Girard, E., Medjoubi, K., Dhaussy, A.-C. & Kahn, R. (2012). *J. Appl. Cryst.* **45**, 652–661.
Garman, E. F. (2010). *Acta Cryst.* D**66**, 339–351.
Garman, E. & Nave, C. (2002). *J. Synchrotron Rad.* **9**, 327–328.
Henderson, R. (1990). *Proc. R. Soc. London Ser. B*, **241**, 6–8.
Hendrickson, W. A. (1976). *J. Mol. Biol.* **106**, 889–893.
Holton, J. M. (2009). *J. Synchrotron Rad.* **16**, 133–142.
Homer, C., Cooper, L. & Gonzalez, A. (2011). *J. Synchrotron Rad.* **18**, 338–345.
Hope, H. (1988). *Acta Cryst.* B**44**, 22–26.
Kmetko, J., Husseini, N. S., Naides, M., Kalinin, Y. & Thorne, R. E. (2006). *Acta Cryst.* D**62**, 1030–1038.
Liebschner, D., Dauter, M., Rosenbaum, G. & Dauter, Z. (2012). *Acta Cryst.* D**68**, 1430–1436.
McMaster, W. H., Kerr Del Grande, N., Mallett, J. H. & Hubbel, J. H. (1969). *Periodic Table: X-ray Properties*. http://www.csrri.iit.edu/periodic-table.html.
Otwinowski, Z. & Minor, W. (1997). *Methods Enzymol.* **276**, 307–326.
Owen, R. L., Rudiño-Piñera, E. & Garman, E. F. (2006). *Proc. Natl Acad. Sci. USA*, **103**, 4912–4917.
Paithankar, K. S., Owen, R. L. & Garman, E. F. (2009). *J. Synchrotron Rad.* **16**, 152–162.
Ravelli, R. B. G. & Garman, E. F. (2006). *Curr. Opin. Struct. Biol.* **16**, 624–629.
Ravelli, R. B. G. & McSweeney, S. M. (2000). *Structure*, **8**, 315–328.
Rodgers, D. W. (1994). *Structure*, **2**, 1135–1140.
Rosenbaum, G. *et al.* (2006). *J. Synchrotron Rad.* **13**, 30–45.
Shimizu, N., Hirata, K., Hasegawa, K., Ueno, G. & Yamamoto, M. (2007). *J. Synchrotron Rad.* **14**, 4–10.
Sliz, P., Harrison, S. C. & Rosenbaum, G. (2003). *Structure*, **11**, 13–19.
Warkentin, M., Hopkins, J. B., Badeau, R., Mulichak, A. M., Keefe, L. J. & Thorne, R. E. (2013). *J. Synchrotron Rad.* **20**, 7–13.

Warkentin, M. & Thorne, R. (2010). *J. Struct. Funct. Genomics*, **11**, 85–89.

Weik, M., Ravelli, R. B. G., Kryger, G., McSweeney, S., Raves, M. L., Harel, M., Gros, P., Silman, I., Kroon, J. & Sussman, J. L. (2000). *Proc. Natl Acad. Sci. USA*, **97**, 623–628.

Weiss, M. S., Panjikar, S., Mueller-Dieckmann, C. & Tucker, P. A. (2005). *J. Synchrotron Rad.* **12**, 304–309.

Zeldin, O. B., Brockhauser, S., Bremridge, J., Holton, J. M. & Garman, E. F. (2013). *Proc. Natl Acad. Sci. USA*, **110**, 20551–20556.